Lattice Boltzmann simulation of nonequilibrium effects in oscillatory gas flow

G. H. Tang,* X. J. Gu, R. W. Barber, and D. R. Emerson
Computational Science and Engineering Department, STFC Daresbury Laboratory, Warrington, WA4 4AD, United Kingdom

Y. H. Zhang†
Department of Mechanical Engineering, University of Strathclyde, Glasgow, G1 1XJ, United Kingdom

(Received 22 April 2008; revised manuscript received 14 July 2008; published 19 August 2008)

Accurate evaluation of damping in laterally oscillating microstructures is challenging due to the complex flow behavior. In addition, device fabrication techniques and surface properties will have an important effect on the flow characteristics. Although kinetic approaches such as the direct simulation Monte Carlo (DSMC) method and directly solving the Boltzmann equation can address these challenges, they are beyond the reach of current computer technology for large scale simulation. As the continuum Navier-Stokes equations become invalid for nonequilibrium flows, we take advantage of the computationally efficient lattice Boltzmann method to investigate nonequilibrium oscillating flows. We have analyzed the effects of the Stokes number, Knudsen number, and tangential momentum accommodation coefficient for oscillating Couette flow and Stokes' second problem. Our results are in excellent agreement with DSMC data for Knudsen numbers up to $\mathrm{Kn}=\mathcal{O}(1)$ and show good agreement for Knudsen numbers as large as 2.5. In addition to increasing the Stokes number, we demonstrate that increasing the Knudsen number or decreasing the accommodation coefficient can also expedite the breakdown of symmetry for oscillating Couette flow. This results in an earlier transition from quasi-steady to unsteady flow. Our paper also highlights the deviation in velocity slip between Stokes' second problem and the confined Couette case.

DOI: 10.1103/PhysRevE.78.026706 PACS number(s): 05.10.−a, 47.61.−k, 47.45.−n

I. INTRODUCTION

Oscillating microstructures are commonly used in modern technology, e.g., microaccelerometers, inertial sensors, and resonant filters [1–3]. Evaluation of the damping forces in these miniaturized devices is difficult because of the complex flow behavior. In addition to viscous and unsteady effects, it is necessary to consider nonequilibrium phenomena. In this paper, we focus on understanding how nonequilibrium and gas-surface interactions will affect the behavior of time-periodic shear-driven gas flows in oscillating microstructures.

The departure from equilibrium is characterized by the Knudsen number (Kn), defined as the ratio of the molecular mean free path λ to the characteristic length L. In general, the Navier-Stokes equations with no-velocity-slip and no-temperature-jump wall conditions are only appropriate when $\mathrm{Kn}<0.001$. However, the gas flow in micro and nanofluidic devices is often in the slip ($0.001<\mathrm{Kn}<0.1$) or the transition regime ($0.1<\mathrm{Kn}<10$). The direct simulation Monte Carlo (DSMC) method can be employed to investigate the flow physics in such unsteady nonequilibrium microflows and important results of oscillatory flow characteristics have been achieved [4–6]. Unfortunately, the statistical scattering and computational requirements (memory and CPU) makes DSMC inefficient, especially for low-speed, low-Kn flows. Direct solution of the Boltzmann equation offers an alternative kinetic approach that can provide an accurate description of nonequilibrium flow [7–10]. However, due to the inherent nonlinearity, complexity of the collision integral, and the multidimensionality of the equation, present solutions are limited to relatively simple geometries. In contrast to kinetic methods, continuum-based models with slip boundary conditions, though simple and convenient, fail to predict critical flow characteristics in the Knudsen layer, which extends a few molecular mean free paths away from the wall [8,11–16]. Within this layer, the linear constitutive relationships for shear stress and heat flux, as assumed in the Navier-Stokes-Fourier equations, are no longer valid [17].

A new computationally efficient method is required to investigate damping forces in micro and nano oscillating devices. Ideally, the method should have an accuracy that is comparable to DSMC or direct solution of the Boltzmann equation. In this paper, we introduce such a method—the lattice Boltzmann (LB) model—to investigate nonequilibrium oscillatory gas flows. Due to its intrinsically kinetic nature, the LB approach has recently attracted considerable research interest for modeling nonequilibrium gas flow [18–34]. Compared to other kinetic methods, the LB model has a significantly lower computational cost and allows convenient treatment of complex geometries. In addition, the lattice Boltzmann model does not suffer from the closure and boundary condition problems associated with higher-order continuum approaches such as Grad's method of moments [35]. More recently, higher-order LB models [36–38] and LB models incorporating the wall effect on the local mean free path [16,30,33,39] have captured the nonlinear behavior of the stress and heat flux in the Knudsen layer. However, to the best of the authors' knowledge, the lattice Boltzmann model has not been applied to oscillatory nonequilibrium flows. Since the LB method is second-order accurate in space and time, it belongs to the family of explicit, second-order time-marching schemes [40,41]. It can capture the time evolution

*g.tang@dl.ac.uk
†yonghao.zhang@strath.ac.uk

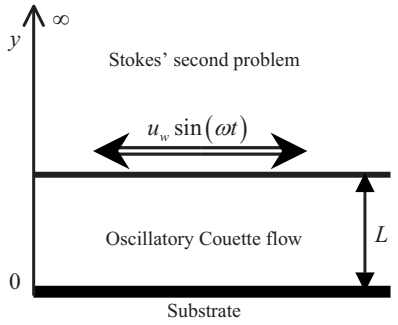

FIG. 1. Schematic diagram of the oscillatory flow cases: confined Couette flow occurs between the stationary substrate at $y=0$ and the oscillating plate, located at $y=L$, whereas the semi-infinite Stokes' second problem propagates into the unbounded medium above $y=L$.

naturally without any additional iteration and is therefore a very effective computational method for describing unsteady nonequilibrium flows.

In this paper, we extend the LB model by incorporating the wall effect on the local mean free path, as discussed in previous work [16]. We then investigate unsteady nonequilibrium Couette flow between two infinite parallel plates and compare the results with available DSMC data. After evaluating our model's performance, we study the dynamic behavior of oscillating Couette flow and Stokes' second problem, which is associated with an unbounded gas above an oscillating plate.

II. NONEQUILIBRIUM LATTICE BOLTZMANN MODEL

We consider a planar Couette flow consisting of a stationary lower plate at $y=0$ and a moving upper plate at $y=L$, with both plates maintained at the same temperature T. The upper plate oscillates harmonically in the lateral direction with velocity $u=u_w \sin(\omega t)$, as illustrated in Fig. 1, where ω is the oscillatory frequency and u_w is the velocity amplitude of the oscillating plate. The oscillatory flow can be characterized by the Stokes' number β, which represents the balance between the unsteady and viscous effects, and can be defined by

$$\beta = \sqrt{\frac{\omega L^2}{\nu_0}}, \tag{1}$$

where ν_0 is the kinematic viscosity of the gas.

The evolution equation for the lattice Bhatnagar-Gross-Krook (BGK) model is given by [42]

$$\frac{\partial f_k}{\partial t} + e_{ki}\frac{\partial f_k}{\partial x_i} = -\frac{f_k - f_k^{eq}}{\phi}, \tag{2}$$

where f_k is the velocity distribution function, f_k^{eq} is the distribution function at equilibrium, e_{ki} is the lattice velocity, and ϕ is the relaxation time. After discretizing Eq. (2), we obtain

$$f_k(\mathbf{x}+\mathbf{e}_k\delta t, t+\delta t) - f_k(\mathbf{x},t) = -\frac{1}{\tau}[f_k(\mathbf{x},t) - f_k^{eq}(\mathbf{x},t)], \tag{3}$$

where $\tau=\phi/\delta t$ is the nondimensional relaxation time and δt is the time step.

For a two-dimensional, thirteen-velocity lattice model (D2Q13) [39], the equilibrium distribution function can be expressed as

$$f_k^{eq} = \rho\omega_k\left[1 + \frac{e_{ki}u_i}{c_s^2} + \frac{(e_{ki}u_i)^2}{2c_s^4} - \frac{u_i u_i}{2c_s^2} + \frac{(e_{ki}u_i)^3}{2c_s^6} - \frac{3(e_{ki}u_i)(u_i u_i)}{2c_s^4}\right],$$

$$\omega_0 = \frac{3}{8}, \quad \omega_k = \frac{1}{12}, \quad k = 1-4, \quad \omega_k = \frac{1}{16}, \quad k = 5-8,$$

$$\omega_k = \frac{1}{96}, \quad k = 9-12, \tag{4}$$

where c_s is the sound speed of the lattice fluid, ρ is the density, and u_i is the macroscopic velocity. The sound speed is given by $c_s^2=c^2/2$, where $c=\sqrt{2RT}$ and R is the gas constant. The lattice velocities, e_k, are given by

$$e_0 = 0,$$

$$e_k = \left[\cos\left(\frac{(k-1)\pi}{2}\right), \sin\left(\frac{(k-1)\pi}{2}\right)\right]c, \quad k = 1-4,$$

$$e_k = \left[\cos\left(\frac{(k-5)\pi}{2} + \frac{\pi}{4}\right), \sin\left(\frac{(k-5)\pi}{2} + \frac{\pi}{4}\right)\right]\sqrt{2}c, \quad k = 5-8,$$

$$e_k = \left[\cos\left(\frac{(k-1)\pi}{2}\right), \sin\left(\frac{(k-1)\pi}{2}\right)\right]2c, \quad k = 9-12. \tag{5}$$

In the absence of wall effects, we can establish a relationship between the mean free path and the relaxation time

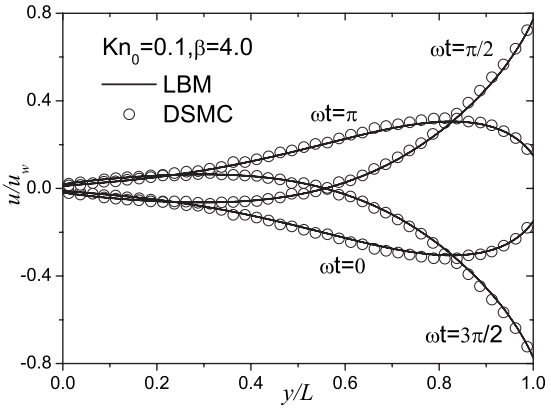

FIG. 2. Dynamic velocity profiles for $Kn_0=0.1$ and $\beta=4.0$ where the symbols represent the DSMC data obtained from Hadjiconstantinou [8]. The stationary and oscillating plates are located at $y/L=0$ and 1, respectively.

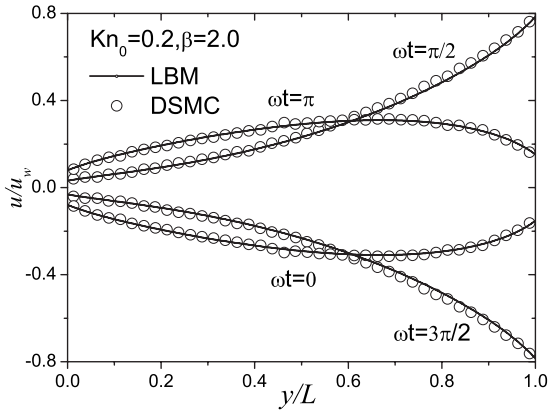

FIG. 3. Dynamic velocity profiles for $\mathrm{Kn}_0=0.2$ and $\beta=2.0$, where the symbols represent the DSMC data obtained from Hadjiconstantinou [8].

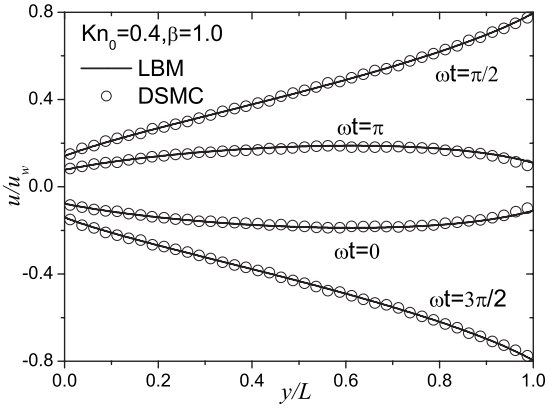

FIG. 4. Dynamic velocity profiles for $\mathrm{Kn}_0=0.4$ and $\beta=1.0$, where the symbols represent the DSMC data obtained from Hadjiconstantinou [8].

based on kinetic theory, i.e., $\lambda_0=(\tau-\frac{1}{2})\delta y\sqrt{\frac{8}{\pi}}\frac{c_s}{c}$ [30]. Therefore, for a D2Q13 lattice BGK model, the *local* relaxation time can be determined by introducing the local mean free path, which takes into account the effect of the wall as follows:

$$\tau=\frac{\lambda}{\lambda_0}\sqrt{\frac{\pi}{8}}\frac{c}{c_s}\mathrm{Kn}_0 N_L+\frac{1}{2}, \tag{6}$$

where $N_L=L/\delta y$ is the number of lattices over the characteristic length, δy is the lattice spacing, and Kn_0 is the Knudsen number based on the mean free path λ_0 evaluated from $\lambda_0=(\mu_0/p)\sqrt{\pi RT/2}$, where p is the pressure and μ_0 is the dynamic viscosity. Molecular gas-wall interactions are important in rarefied flows and geometrical effects on the spatial variation of the local mean free path need to be taken into account [43,44]. By considering the molecular interactions close to the wall, we have established a relationship between the *local* mean free path λ and the macroscopic property-based mean free path λ_0. If we consider an ideal gas bounded by two parallel plates at $y=0$ and $y=L$, the *local* mean free path of the molecules at a distance y $(0<y<L)$ from the lower plate can be calculated as follows [16]:

$$\lambda(y)=\lambda_0\left[1+(\xi-1)\exp(-\xi)-\xi^2\int_{\xi}^{\infty}t^{-1}\exp(-t)dt\right], \tag{7}$$

where $\xi=y/\lambda_0$ for those molecules moving towards $y=0$ and $\xi=(L-y)/\lambda_0$ for those moving towards $y=L$. Since a molecule can move towards the two walls with equal probability, the *local* mean free path of all molecules in the flow domain can be determined by averaging these two parts. For $y=0$ or $y=L$, we have $\xi=L/\lambda_0$.

To capture the slip velocity at the wall, the Maxwellian kinetic boundary condition accounting for the tangential momentum accommodation coefficient is employed [26,45]. The unknown reflected distribution function f_k on the wall can be determined from the incident distribution function $f_{k'}$ as follows:

$$f_k(\mathbf{x},t+\delta t)=(1-\alpha)f_{k'}(\mathbf{x},t+\delta t)|(\mathbf{e}_{k'}-\mathbf{u}_{wall})\cdot\mathbf{n}|+\alpha\frac{\Sigma_{(\mathbf{e}_i-\mathbf{u}_{wall})\cdot\mathbf{n}<0}|(\mathbf{e}_i-\mathbf{u}_{wall})\cdot\mathbf{n}|f_i(\mathbf{x},t+\delta t)}{\Sigma_{(\mathbf{e}_j-\mathbf{u}_{wall})\cdot\mathbf{n}>0}|(\mathbf{e}_j-\mathbf{u}_{wall})\cdot\mathbf{n}|f_j^{eq}(\mathbf{x},\rho_{wall},\mathbf{u}_{wall})}f_k^{eq}(\mathbf{x},\rho_{wall},\mathbf{u}_{wall}), \tag{8}$$

where $\mathbf{u}_{wall}$ and ρ_{wall} are the velocity and density at the wall, respectively, and $\mathbf{n}$ is the unit normal. The tangential momentum accommodation coefficient α, represents the fraction of impinging molecules absorbed and reemitted diffusely, while $(1-\alpha)$ is the fraction of molecules reflected specularly from the surface. For fully diffuse reflection at the wall, $\alpha=1$.

In the simulations, the oscillation frequency ω is calculated from $\omega=2\pi/(T_p\delta t)$, where T_p represents the period of the imposed oscillatory velocity normalized by δt. The local kinematic viscosity in the D2Q13 lattice BGK model was calculated from $\nu=(\tau-0.5)c_s^2\delta t$.

III. OSCILLATORY COUETTE FLOW

A. Dynamic velocity profiles

Figures 2–4 compare the dynamic velocity profiles from the present lattice Boltzmann model (LBM) against the DSMC data presented by Hadjiconstantinou [8]. The results show that inertial effects become significant as the oscillation

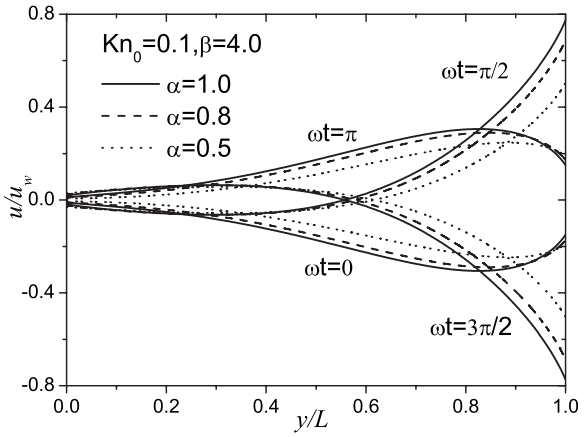

FIG. 5. Dynamic velocity profiles for $Kn_0=0.1$ and $\beta=4.0$ showing the effect of the tangential momentum accommodation coefficient.

frequency increases. It can be seen that both the bulk flow velocity and the velocity in the Knudsen layer are in excellent agreement with DSMC results indicating that the proposed LB model can successfully capture the characteristics of the Knudsen layer in unsteady flows. Figure 5 illustrates the effect of the tangential momentum accommodation coefficient on the dynamic velocity profiles and indicates that the slip velocity increases as the value of α decreases.

B. Velocity history

Figure 6 shows the history of the streamwise velocity at various locations between the stationary and oscillating plates for $Kn_0=1.0$. In Fig. 6(a), which shows a typical quasisteady flow behavior, it can be seen that the velocity amplitude increases as $y/L\rightarrow 1$, i.e., as we approach the oscillating plate. However, at higher Stokes numbers, as shown in Fig. 6(b), the time history exhibits a more complex pattern because the velocity amplitude decays rapidly away from the moving wall. In contrast, the phase lag can be seen to grow as we move further away from the oscillating wall. The results illustrate that the phase difference between the velocity signal imposed on the oscillating wall and the signal felt at the stationary wall increases with Stokes number β. However, as shown in Fig. 7, increasing the Knudsen number has only a small effect on the phase difference between the oscillating and stationary walls. Comparing the results from our LB model against the DSMC data presented by Bahukudumbi *et al.* [13] shows that the proposed lattice Boltzmann model provides satisfactory results for Knudsen numbers as large as 2.5.

Figure 8 presents the velocity distribution for a Stokes number of $\beta=5$. It can be seen that the phase difference between the velocity signals at the various locations becomes significant demonstrating the importance of inertial effects as the oscillation frequency increases. We also compare our results with the analytical slip-flow solution of the Navier-Stokes equations given by Park *et al.* [15]. The deviations at the walls are largely due to the fact that the analytical solution does not take account of the Knudsen layers. We have

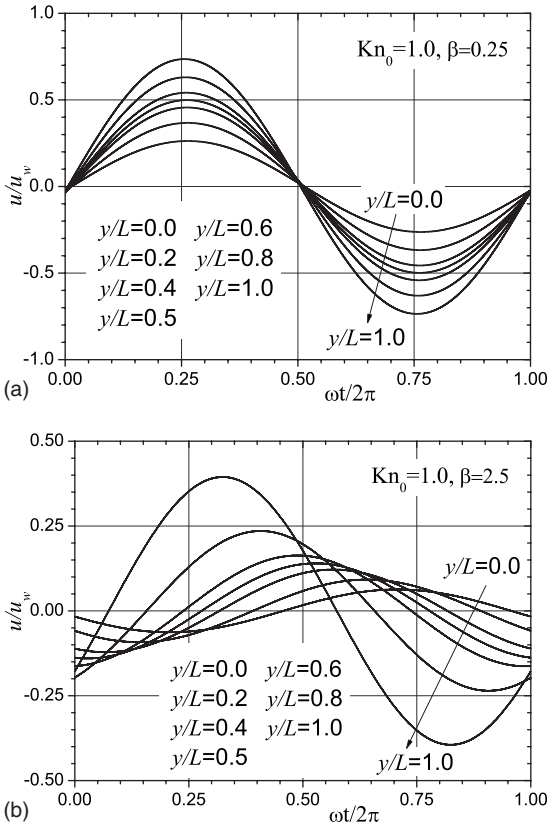

FIG. 6. Streamwise velocity history for $Kn_0=1.0$, and (a) $\beta=0.25$; (b) $\beta=2.5$, where the stationary and oscillating plates are located at $y/L=0$ and 1, respectively.

also investigated the effect of the tangential momentum accommodation coefficient for high Stokes number flows. Figure 9 shows the streamwise velocity history for $\beta=5.0$ and $Kn_0=0.1$ for values of α ranging from 0.5 to 1.0. As the accommodation coefficient decreases, the phase lag increases in comparison to the no-slip continuum solution.

C. Velocity amplitude

Figures 10 and 11 show the velocity amplitude between the two surfaces normalized by u_w. The LB results are again in very good agreement with the DSMC data given by Park *et al.* [15]. Although the cases for $\beta\leqslant 0.25$ are usually classified as quasisteady flow [15], Figure 10 indicates that the velocity profile can lose its symmetry if the Knudsen number is sufficiently large. When the Knudsen number increases, the gas becomes more dilute so that the frequency of collisions between the gas molecules is reduced. It therefore takes longer to transfer momentum from the oscillating plate which leads to an earlier transition from a quasisteady state to an unsteady flow condition. Figure 11 shows the effect of increasing the Stokes number when the Knudsen number is fixed. For $\beta=0.25$ and 1.0, the velocity amplitudes are very similar. However, for higher Stokes numbers, the deviation from the symmetrical velocity profile becomes significant and the slip velocity at the stationary wall is much smaller than that at the oscillating wall. In addition, as the Stokes number is increased, the slip velocity at the stationary wall

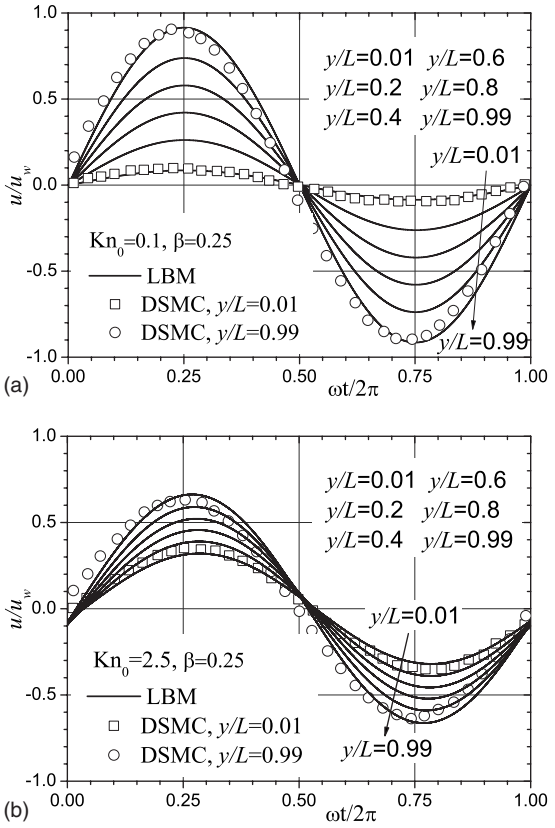

FIG. 7. Streamwise velocity history for $\beta=0.25$ and (a) $\mathrm{Kn}_0=0.1$; (b) $\mathrm{Kn}_0=2.5$. The symbols represent the DSMC data at two locations with $y/L=0.01$ and 0.99 given by Bahukudumbi *et al.* [13].

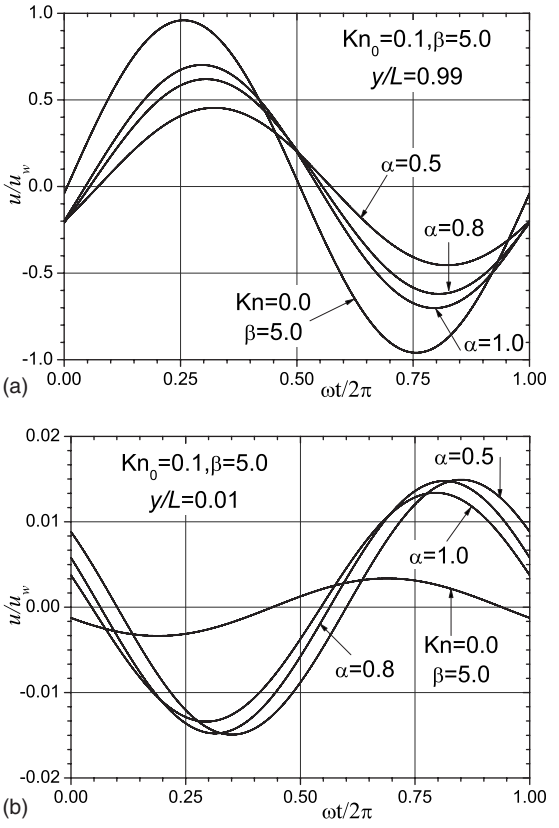

FIG. 9. Streamwise velocity history for different accommodation coefficients at $\mathrm{Kn}_0=0.1$, $\beta=5.0$, and (a) $y/L=0.99$; (b) $y/L=0.01$. The results for a continuum flow with $\mathrm{Kn}=0$ is presented for comparison.

decreases whilst the slip at the oscillating wall increases. Figure 11 shows that when the Stokes number is large, the flow is confined to a near-wall region or bounded Stokes' layer [15].

Figure 12 shows the effect of the Knudsen number on the velocity amplitude at moderate and high Stokes numbers.

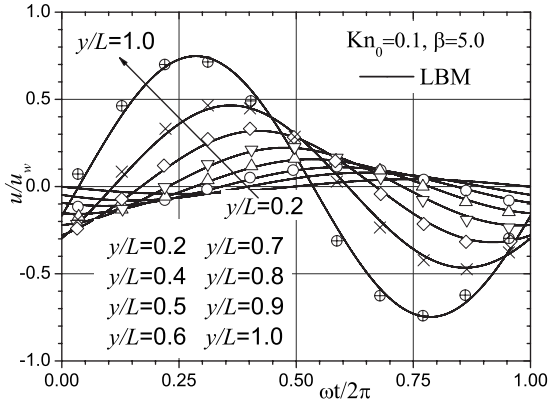

FIG. 8. Streamwise velocity history for $\mathrm{Kn}_0=0.1$ and $\beta=5.0$, where y/L indicates the distance from the stationary plate $y/L=0$. The oscillating plate is located at $y/L=1$. The symbols represent the analytical solution of the Navier-Stokes equations given by Park *et al.* [15]: ○, $y/L=0.5$; △, $y/L=0.6$; ▽, $y/L=0.7$; ◇, $y/L=0.8$; ×, $y/L=0.9$; ⊕, $y/L=1.0$.

The quasisteady flow description is still appropriate for the case of $\beta=1.0$ and $\mathrm{Kn}_0=0.1$ because the velocity amplitude remains symmetrical. However, quasisteady flow breaks down when the Knudsen number reaches 0.5, as can be clearly seen in Fig. 12(a). Although the magnitude of the slip velocity at the oscillating plate increases with the Knudsen number, a more complicated behavior is exhibited at the stationary plate. The results also show that the transition from quasisteady flow to unsteady flow occurs at a modest Stokes

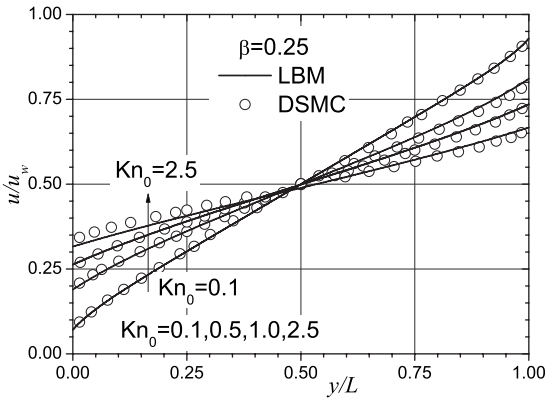

FIG. 10. Streamwise velocity amplitude at various Knudsen numbers for $\beta=0.25$. The symbols represent the DSMC data given by Park *et al.* [15].

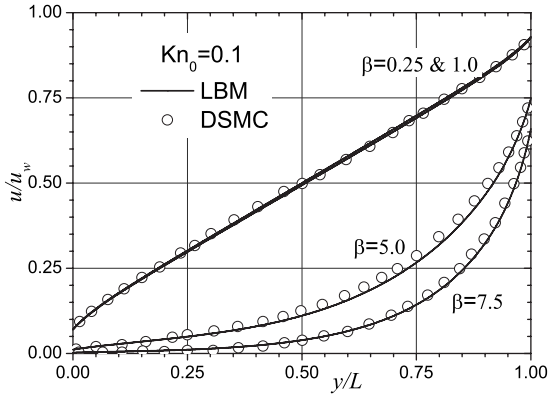

FIG. 11. Streamwise velocity amplitude at various Stokes numbers for $Kn_0=0.1$. The symbols represent the DSMC data given by Park *et al.* [15].

number for highly nonequilibrium flows. From Figs. 11 and 12, it can be seen that the Stokes number rather than the Knudsen number is important in determining the thickness of the bounded Stokes layer. Conversely, the Knudsen number is more important than the Stokes number in determining the velocity slip at the oscillating wall. We have also examined the effect of the accommodation coefficient α and have found that the flow experiences an earlier transition from quasisteady to unsteady conditions as the accommodation coefficient is decreased. Even at small Stokes numbers, reducing the accommodation coefficient can expedite the

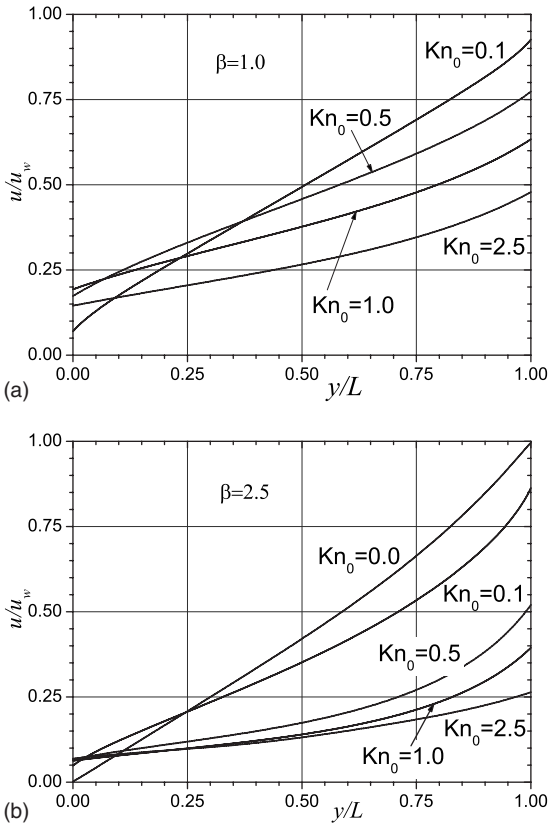

FIG. 12. Streamwise velocity amplitude at various Knudsen numbers: (a) $\beta=1.0$. (b) $\beta=2.5$.

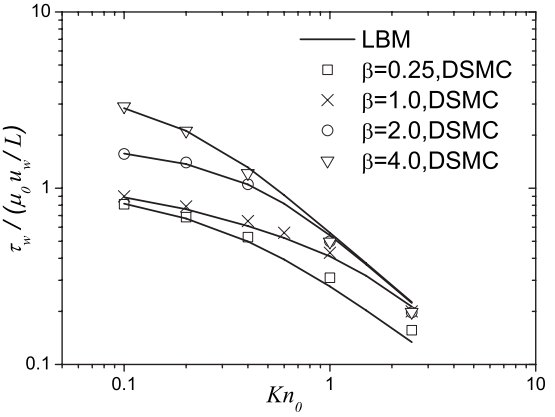

FIG. 13. Shear stress on the oscillating plate as a function of the Knudsen number. The symbols represent the DSMC data given by Hadjiconstantinou [8].

breakdown of the symmetrical velocity distribution. When the tangential momentum accommodation coefficient decreases, the amount of slip at the plates will increase, as illustrated in Fig. 9. In addition, the phase lag will increase and the gas becomes less responsive to the plate oscillation, effectively increasing the inertia of the system.

D. Shear stress

In contrast to Navier-Stokes approaches, it is convenient to evaluate the shear stress independently of the velocity fields in lattice Boltzmann models. This is because the LB method is kinetic in nature and the shear stress can be computed directly from the distribution function. Figure 13 shows the predicted shear stress on the oscillating wall, normalized by the continuum limit for steady planar Couette flow, $\tau_w=\mu_0 u_w/L$. As the Stokes number increases, the wall shear stress increases especially at low Knudsen numbers. Good agreement is observed between our LB results and the DSMC data given by Hadjiconstantinou [8] for Knudsen numbers as large as 2.5.

IV. COMPARISON OF OSCILLATING COUETTE FLOW AND STOKES' SECOND PROBLEM

In practical applications involving laterally oscillating plates, not only should the damping force between the two parallel plates be accounted for but also the damping due to the ambient gas above the oscillating plate. It is informative, therefore, to compare the dynamic behavior of confined Couette flow with Stokes' second problem, which considers the motion of an unbounded gas above an oscillating flat plate.

To simulate Stokes' second problem, we applied a stationary wall condition at $y=10L$. In addition, we adopted an extrapolation scheme to obtain the unknown distribution function at the upper boundary which was placed sufficiently far away from the oscillating plate to have a negligible influence on the flow field. Figure 14 shows the dynamic velocity profiles for both the confined and unconfined cases at intervals of $\omega t=\pi/4$ over half a period. The presented velocity profile above the oscillating plate is a strongly damped

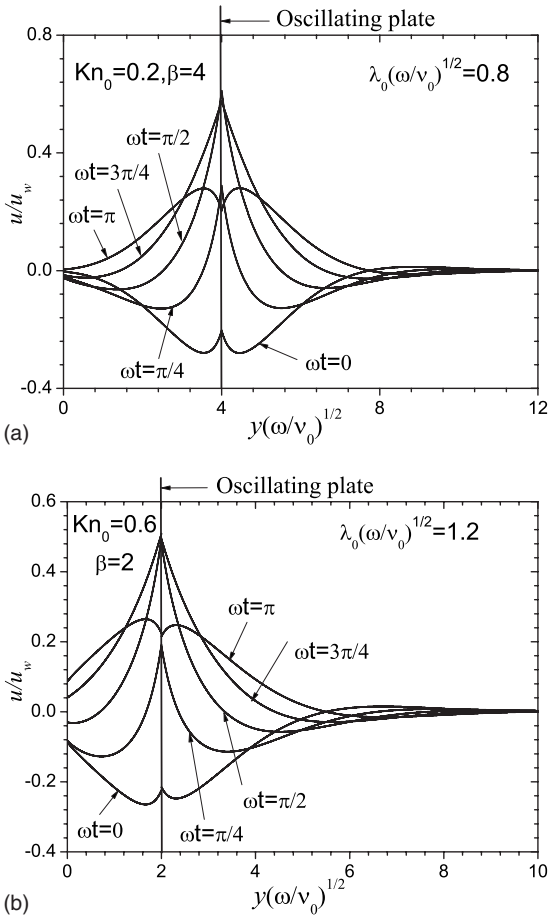

FIG. 14. Dynamic velocity profiles for confined Couette flow and Stokes' second problem. The location of the oscillating plate is indicated by a vertical solid line at (a) $y(\omega/\nu_0)^{1/2}=4$ and (b) $y(\omega/\nu_0)^{1/2}=2$. The stationary plate is located at $y(\omega/\nu_0)^{1/2}=0$. Oscillatory Couette flow occurs between the stationary and moving plates whilst Stokes' second problem propagates away from the oscillating plate into the unbounded region.

oscillation of exponentially decaying amplitude. The velocity is negligible beyond the penetration depth, which is defined as the distance above the moving plate where the amplitude of the oscillation has decreased to one percent of the wall velocity u_w. In Stokes' second problem, the rarefaction is usually characterized by defining the Knudsen number as $\lambda_0\sqrt{\omega/\nu_0}$. Figure 14 shows that the velocity profiles on both sides of the oscillating plate are similar up to $\mathrm{Kn}_0=0.2$ but start to show differences as the Knudsen number continues to increase. This is confirmed in Fig. 15, which shows the velocity amplitude for both the confined and unbounded cases. It can be seen that the slip velocity either side of the oscillating plate starts to differ when the Knudsen number approaches $\mathrm{Kn}_0=0.6$. This can be explained by the fact that the Knudsen layers at the stationary and oscillating plates start to

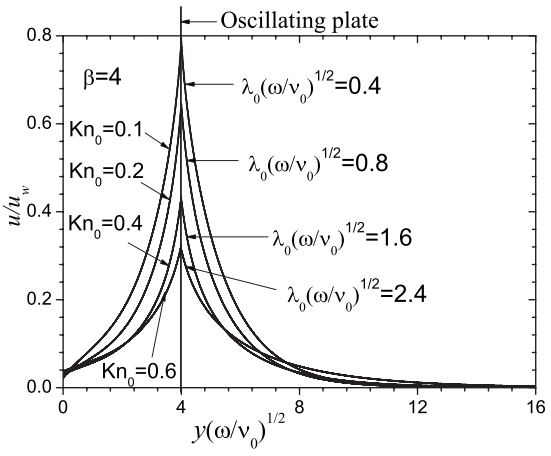

FIG. 15. Velocity amplitude showing the effect of the Knudsen number on Couette flow and Stokes' second problem. The vertical solid line at $y(\omega/\nu_0)^{1/2}=4$ represents the location of the oscillating plate.

overlap when the Knudsen number exceeds 0.5. In previous studies, this Knudsen layer interference has usually been ignored.

V. CONCLUSIONS

The nonequilibrium flow characteristics in laterally oscillating structures have been investigated using an extended lattice Boltzmann model that can account for the effects of the Knudsen layer. We first investigate oscillatory Couette flow between two infinite parallel plates. The lattice Boltzmann model is shown to be in very good agreement with available DSMC data for Knudsen numbers up to ~2.5. Increasing the Stokes number and the Knudsen number or decreasing the tangential momentum accommodation coefficient is shown to lead to an earlier transition from quasisteady to unsteady flow. We then compare the dynamic behavior of confined Couette flow with Stokes' second problem. Our model is able to account for the overlapping Knudsen layers in the Couette problem and can capture the deviation in slip velocity between the confined and unbounded cases. The study demonstrates that the lattice Boltzmann model is a very effective computational method for describing unsteady nonequilibrium flows.

ACKNOWLEDGMENTS

The authors are grateful for the helpful discussions with Professor Jason Reese at the University of Strathclyde. This work was financially supported by the UK Engineering and Physical Sciences Research Council (EPSRC) under Grant No. EP/D07455X/1. Additional support was provided by EPSRC under the auspices of Collaborative Computational Project 12.

[1] Y. H. Cho, A. P. Pisano, and R. T. Howe, J. Microelectromech. Syst. **3**, 81 (1994).
[2] T. Veijola, H. Kuisma, J. Lahdenpera, and T. Ryhanen, Sens. Actuators, A **48**, 239 (1995).
[3] W. J. Ye, X. Wang, W. Hemmert, D. Freeman, and J. White, J. Microelectromech. Syst. **12**, 557 (2003).
[4] S. Stefanov, P. Gospodinov, and C. Cercignani, Phys. Fluids **10**, 289 (1998).
[5] N. G. Hadjiconstantinou and A. L. Garcia, Phys. Fluids **13**, 1040 (2001).
[6] D. R. Emerson, X. J. Gu, S. K. Stefanov, Y. H. Sun, and R. W. Barber, Phys. Fluids **19**, 107105 (2007).
[7] F. Sharipov, W. Marques, and G. M. Kremer, J. Acoust. Soc. Am. **112**, 395 (2002).
[8] N. G. Hadjiconstantinou, Phys. Fluids **17**, 100611 (2005).
[9] F. Sharipov and D. Kalempa, Phys. Fluids **19**, 017110 (2007).
[10] F. Sharipov and D. Kalempa, Microfluid. Nanofluid. **4**, 363 (2008).
[11] T. Veijola and M. Turowski, J. Microelectromech. Syst. **10**, 263 (2001).
[12] T. Veijola, J. Micromech. Microeng. **14**, 1109 (2004).
[13] P. Bahukudumbi, J. H. Park, and A. Beskok, Microscale Thermophys. Eng. **7**, 291 (2003).
[14] O. M. Haddad, M. A. Al-Nimr, and M. M. Abuzaid, Acta Mech. **179**, 249 (2005).
[15] J. H. Park, P. Bahukudumbi, and A. Beskok, Phys. Fluids **16**, 317 (2004).
[16] G. H. Tang, Y. H. Zhang, X. J. Gu, and D. R. Emerson, Europhys. Lett. (to be published).
[17] M. Gad-el-Hak, J. Fluids Eng. **121**, 5 (1999).
[18] Y. H. Zhang, R. S. Qin, and D. R. Emerson, Phys. Rev. E **71**, 047702 (2005).
[19] X. B. Nie, G. D. Doolen, and S. Chen, J. Stat. Phys. **107**, 279 (2002).
[20] C. Y. Lim, C. Shu, X. D. Niu, and Y. T. Chew, Phys. Fluids **14**, 2299 (2002).
[21] G. H. Tang, W. Q. Tao, and Y. L. He, Int. J. Mod. Phys. C **15**, 335 (2004).
[22] X. D. Niu, C. Shu, and Y. T. Chew, Europhys. Lett. **67**, 600 (2004).
[23] G. H. Tang, W. Q. Tao, and Y. L. He, J. Appl. Phys. **97**, 104918 (2005).
[24] T. Lee and C. L. Lin, Phys. Rev. E **71**, 046706 (2005).
[25] Y. H. Zhang, R. S. Qin, Y. H. Sun, R. W. Barber, and D. R. Emerson, J. Stat. Phys. **121**, 257 (2005).
[26] G. H. Tang, W. Q. Tao, and Y. L. He, Phys. Fluids **17**, 058101 (2005).
[27] M. Sbragaglia and S. Succi, Phys. Fluids **17**, 093602 (2005).
[28] F. Toschi and S. Succi, Europhys. Lett. **69**, 549 (2005).
[29] V. Sofonea and R. F. Sekerka, Phys. Rev. E **71**, 066709 (2005).
[30] Y. H. Zhang, X. J. Gu, R. W. Barber, and D. R. Emerson, Phys. Rev. E **74**, 046704 (2006).
[31] Z. L. Guo, T. S. Zhao, and Y. Shi, J. Appl. Phys. **99**, 074903 (2006).
[32] M. Sbragaglia and S. Succi, Europhys. Lett. **73**, 370 (2006).
[33] Y. H. Zhang, X. J. Gu, R. W. Barber, and D. R. Emerson, EPL **77**, 30003 (2007).
[34] L. Szalmás, EPL **80**, 24003 (2007).
[35] X. J. Gu and D. R. Emerson, J. Comput. Phys. **225**, 263 (2007).
[36] R. Zhang, X. Shan, and H. Chen, Phys. Rev. E **74**, 046703 (2006).
[37] X. D. Niu, S. A. Hyodo, T. Munekata, and K. Suga, Phys. Rev. E **76**, 036711 (2007).
[38] I. V. Karlin and S. Ansumali, Phys. Rev. E **76**, 025701(R) (2007).
[39] G. H. Tang, Y. H. Zhang, and D. R. Emerson, Phys. Rev. E **77**, 046701 (2008).
[40] M. B. Reider and J. D. Sterling, Comput. Fluids **24**, 459 (1995).
[41] X. He, G. D. Doolen, and T. Clark, J. Comput. Phys. **179**, 439 (2002).
[42] S. Chen and G. D. Doolen, Annu. Rev. Fluid Mech. **30**, 329 (1998).
[43] D. W. Stops, J. Phys. D: Appl. Phys. **3**, 685 (1970).
[44] Z. L. Guo, B. C. Shi, and C. G. Zheng, EPL **80**, 24001 (2007).
[45] S. Ansumali and I. V. Karlin, Phys. Rev. E **66**, 026311 (2002).